Biomaterials 31 (2010) 4740–4747

Contents lists available at ScienceDirect

Biomaterials

journal homepage: www.elsevier.com/locate/biomaterials

A high-performance VEGF aptamer functionalized polypyrrole nanotube biosensor

Oh Seok Kwon, Seon Joo Park, Jyongsik Jang*

School of Chemical and Biological Engineering, Seoul National University, 599 Gwanangro, Sillim-dong, Gwanak-gu, Seoul 151-742, Republic of Korea

ARTICLE INFO

Article history:
Received 5 February 2010
Accepted 12 February 2010
Available online 12 March 2010

Keywords:
Vascular endothelial cell growth factors (VEGFs)
Aptamer
Biosensor
Field-effect transistors
Conducting polymer

ABSTRACT

In this study, we examined the in *vitro* electrochemical detection of Vascular Endothelial Growth Factor (VEGF) as cancer biomarker using *p*-type field-effect transistor (FET) biosensor. We demonstrated the high-performance FET sensor, which could detect ca. 400 fM of VEGF concentration, based on anti-VEGF RNA aptamer conjugated carboxylated polypyrrole nanotubes (CPNTs). The CPNTs used as high-performance transducers of this FET system were successfully fabricated by cylindrical micelle templates in a water-in-oil emulsion system. The functional carboxyl group (−COOH) was effectively incorporated into the polymer backbone during the polymerization by using pyrrole-3-carboxylic acid (P3CA) as a co-monomer. Two types of CPNTs (CPNT1: ca. 200 nm in diameter, CPNT2: ca. 120 nm in diameter) demonstrated the excellent conductivity performance in this FET system. Based on CPNTs conjugated with anti-VEGF RNA aptamer (CPNTs-aptamer), VEGF (target molecule) acts as the gate dielectrics of *p*-type FET sensor and specifically interacts with anti-VEGF aptamer attached to CPNT surfaces. Importantly, the VEGF detection limit of the FET sensor based on CPNT2-aptamer was found to be near 400 fM in real-time. Moreover, the CPNTs-aptamer FET sensors can be repeatedly used for various concentrations of the target molecule (VEGFs) through the washing and rinsing processes.

1. Introduction

A closed circulatory system for the supply of oxygen and nutrients to all tissues in the body exists in vertebrates; this system develops in early embryogenesis through vasculogenesis and angiogenesis [1]. Recently, angiogenesis has been studied on the molecular mechanisms because it is an important factor to be related to the proliferation and metastasis of cancer cells [2–4]. Among various regulators of angiogenesis, a vascular endothelial growth factor (VEGF) stimulates angiogenesis and lymphangiogenesis by activating VEGF-receptor tyrosine kinases in all endothelial cells [5–8]. VEGF potently promotes angiogenesis and is indispensable for vascular development, making it an attractive target for controlling angiogenic factor that plays a pivotal role in tumor growth and metastasis [9,10]. The abnormally fast growth and division of tumors make it promoted the over-expression of the VEGF because of supply of more nutrients and oxygen, resulting in the induction of tumor lymphatic-vessels and the metastasis of cancer [3]. In this point, VEGF discrimination in blood is a challenging research subject for key applications in fields of clinical diagnoses for cancers. Therefore, a few significant studies regarding detection of VEGF levels in blood have been reported, mainly based on FET biosensor with Si nanowire [11], a fluorescent images [1,12], VEGF receptors [13] and ELISA [14]. However, their easy, rapid detection and high sensitivity are still challenging for improvement.

Aptamers are comprised of an artificial oligonucleic acid or peptide molecule and have high affinity, specificity and selectivity to specific target molecules. Therefore, various aptamers have been utilized for therapeutic and clinical applications [15]. More interestingly, the aptamers can be applied to electrochemical sensor as the immobilization on the surface of a transducer in FET because the aptamers in very small size (ca. 2–4 nm) provide adequate distance required for screening the surplus electrical charge by the mobile carries [16]. Therefore, biosensors with various aptamers such as thrombin aptamers, DNA (RNA)-aptamers and protein-aptamers based on nanomaterials have been designed for detecting a low concentration of bio-molecules [17–19]. However, these biosensors based on the aptamers showed some limitations such as difficulties in controlling the synthesis and modifying the surface of nanomaterials.

Recently, remarkable process in synthesis and characterization of conducting polymer (CP) nanomaterials has offered a great

* Corresponding author. Tel.: +82 2 880 7069; fax: +82 2 8881604.
E-mail address: jsjang@plaza.snu.ac.kr (J. Jang).

0142-9612/$ – see front matter © 2010 Elsevier Ltd. All rights reserved.
doi:10.1016/j.biomaterials.2010.02.040

possibility for novel applications in various fields because of outstanding physical and chemical characteristics originating from their small dimensions and high surface area [20–23]. CP nanomaterials also inherit the facile functionalization and biocompatibility from their bulk counterparts [24,25]. In particular, one-dimensional (1D) CP nanomaterials have emerged as promising candidates for fabricating of state-of-the art devices [26]. 1D CP nanomaterials can minimize the loss in signal intensity by lateral current shunting and offer improved sensitivity through depletion or accumulation of charge carriers on the nanomaterial surfaces when they were used as transducer of field-effect transistor (FET) sensors [27–29]. Although various 1D nanomaterials as the conductive channel of FET-type biosensor have utilized, none of the research performed to data has demonstrated the sensitivity effects through size controlling of conductive channel.

Herein, we developed the FET-type biosensor to detect target molecule (VEGF), which was based on CPNTs conjugated with anti-VEGF RNA aptamer. Binding CPNTs on the FET substrate and immobilizing anti-VEGF RNA aptamer provide the strong affinity between anti-VEGF RNA aptamer and VEGF into a FET-platform suitable for electronic control. Field-induced sensitivities to various VEGF concentrations were observed, eventually leading to the recognition of VEGF at an unprecedentedly low concentration. Moreover, this FET platform can be also re-useable for various concentrations of the target molecule.

2. Experimental

2.1. Materials

Pyrrole (98%) and pyrrole-3-carboxylic acid (P3CA, 95%) were purchased from Aldrich and Acros Organics. Sodium bis(2-ethylhexyl)-sulfosuccinate (AOT; Aldrich, 98%) and hexane (Aldrich, 99%) were obtained from Aldrich. Vascular Endothelial Growth Factor ($VEGF_{165}$) was purchased from Cell Signal Technology, Inc. Anti-VEGF RNA aptamer was purchased from Bioneer Co. (Daejeon, Korea). The aptamer was modified at the 5′-terminus with an amine group and its sequence was as follows: 5′-NH_2-AUG CAG UUU GAG AAG UCG CGC AU-3′. The aptamer stock solution was diluted with diethylpyrocarbonate (DEPC)-treated water and stored in the freezer before use (−20 °C).

2.2. 4-(4,6-Dimethoxy-1,3,5-triazin-2-yl)-4-methyl-morpholinium chloride (DMT-MM)

An efficient condensing agent, DMT-MM, was synthesized according to the procedure described by Kunishima et al. [30]. First, 0.75 g of 2-chloro-4,6-dimethoxy-1,3,5-triazine was reacted with 1 g of *N*-methylmorpholine in 20 mL of tetrahydrofuran (THF) for 30 min. The resulting white precipitates were washed with THF, and then dried. The final product was stored in a freezer under −20 °C. DMT-MM is capable of providing excellent yields in water as well as alcohol phases for the condensation reaction between carboxylic acid and amine groups.

2.3. Fabrication of carboxylated polypyrrole nanotubes (CPNTs)

Carboxylated polypyrrole nanotubes (CPNTs) with two different diameters were fabricated by chemical oxidation copolymerization of pyrrole monomer and P3CA in an AOT reverse emulsion system. In the first stage, 15.8 mmol of AOT was dissolved in hexane (40 mL), and 2 mL of 7 M aq. $FeCl_3$ solution was introduced into the AOT/hexane solution mixture to generate AOT reverse cylindrical micelle

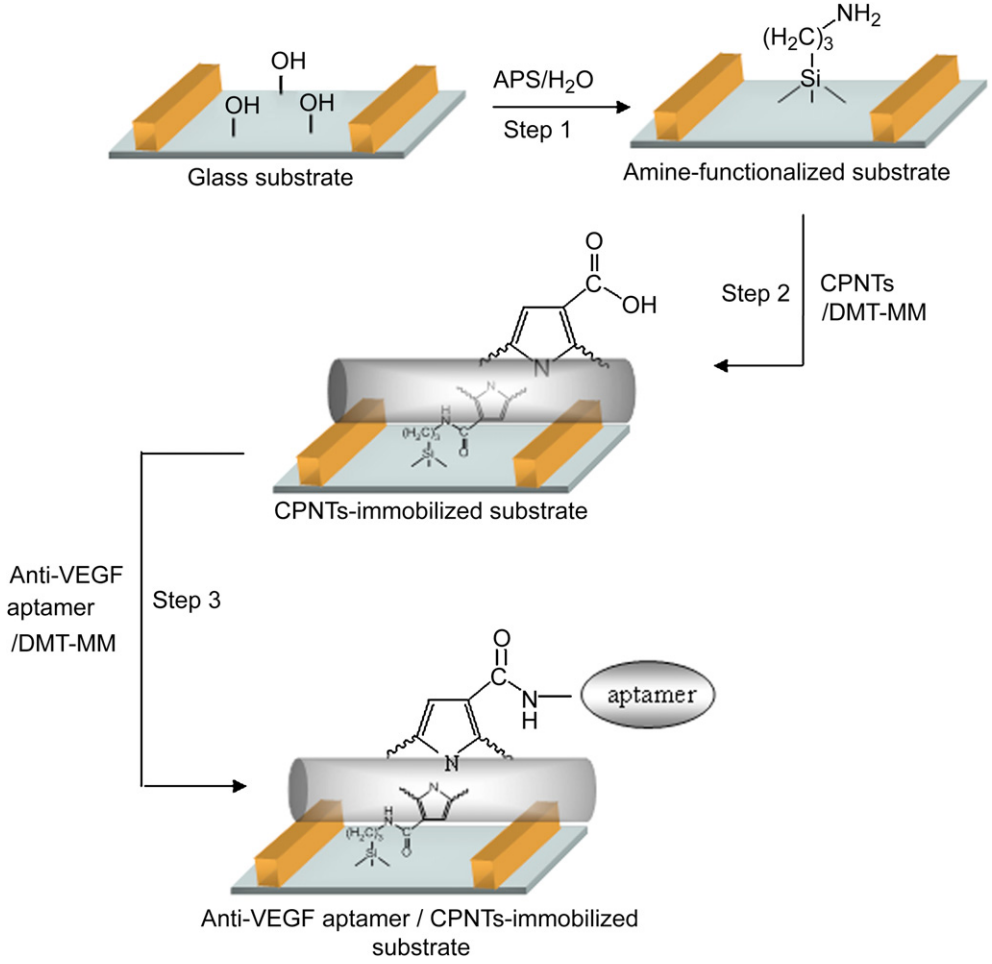

Fig. 1. Schematic illustration of reaction steps for the fabrication of a FET sensor platform based on anti-VEGF aptamer conjugated CPNTs.

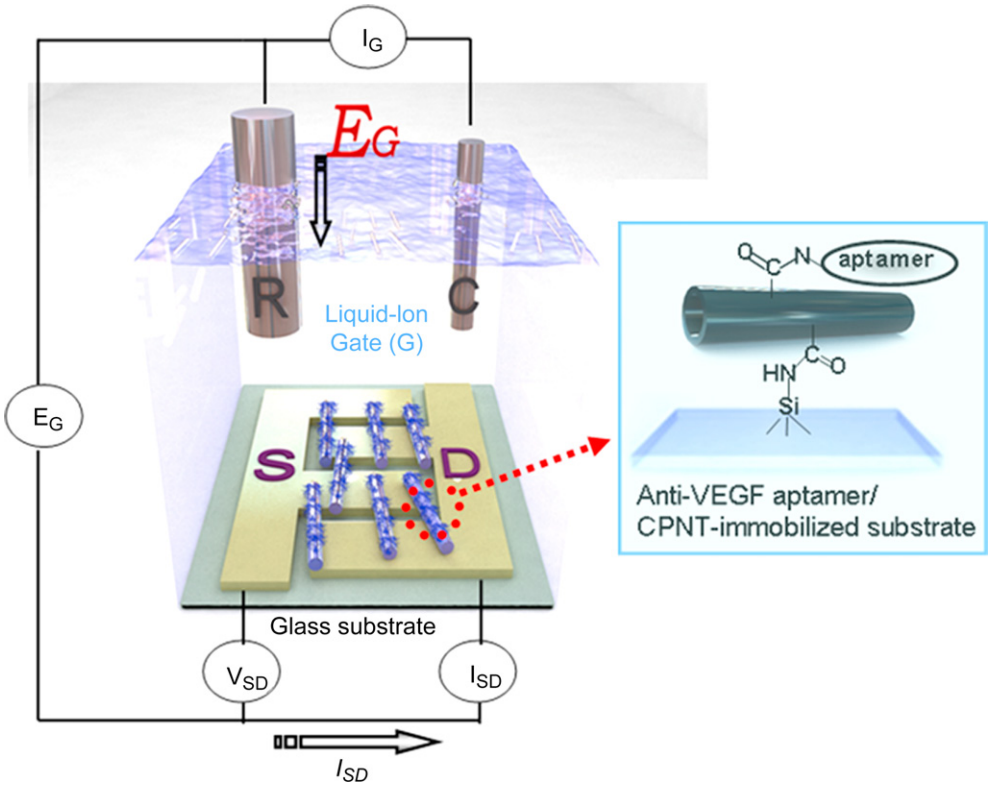

Fig. 2. Illustration of the CPNT-aptamer FET-type sensor configuration used in this work (R: reference electrode, C: counter electrode, S: source and D: drain, G: liquid-ion gate, E_G: gate potential). The FET sensor was consisted with three electrodes system and they were immersed in PBS solution (pH 7.5) as liquid-ion gate. The anti-VEGF aptamer conjugated CPNTs were immobilized on the glass substrate with source and drain electrodes in the liquid-ion gate. The current flows from V_{SD} to I_{SD}.

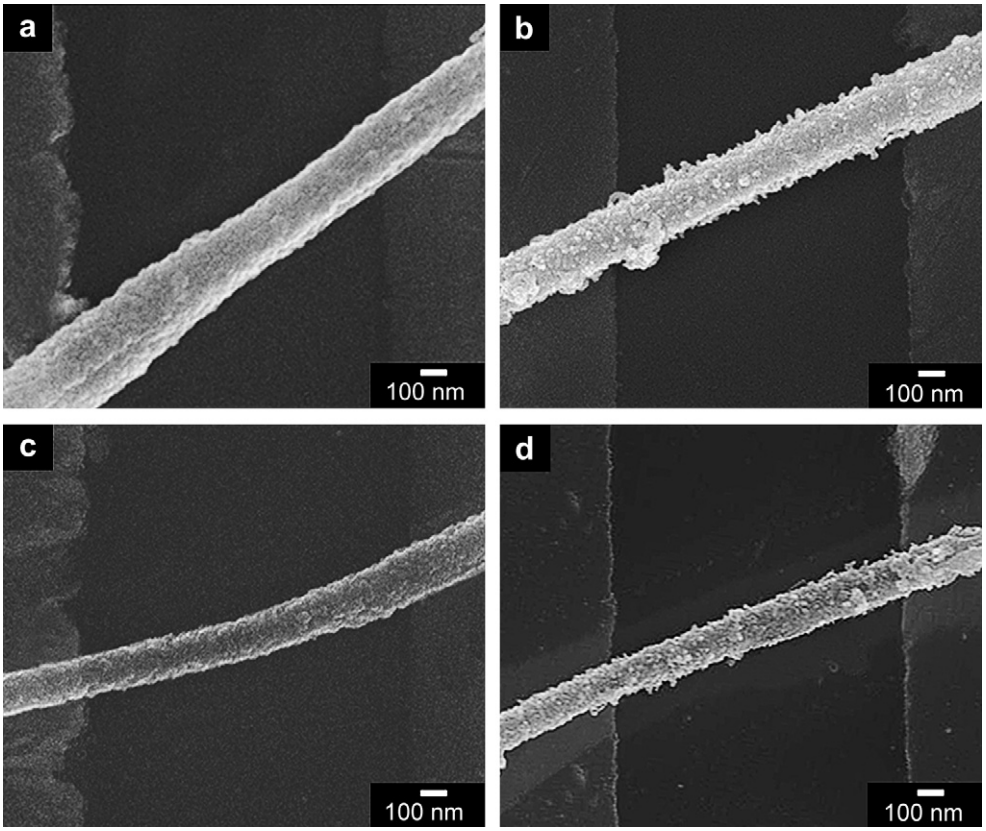

Fig. 3. Typical FE-SEM images of FET sensor platform with CPNTs; (a) and (c) indicate the pristine CPNT1 and CPNT2. (b) and (d) represent CPNT1-aptamer and CPNT2-aptamer after immobilizing the anti-VEGF aptamer on the surface of the CPNTs.

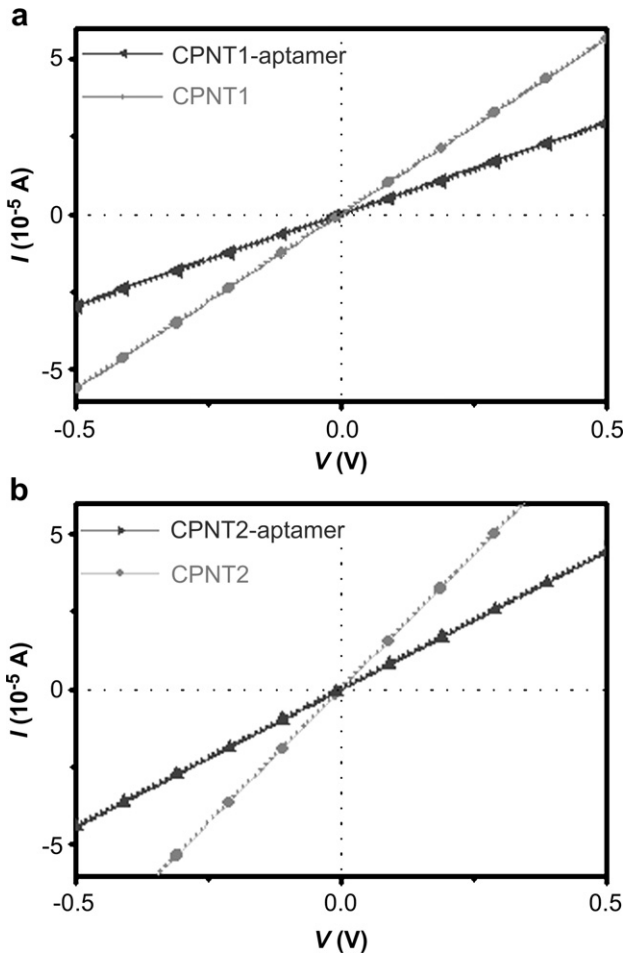

Fig. 4. Current–voltage (I–V) of CPNTs on the electrode substrate before and after introduction of anti-VEGF aptamer into CPNTs in air circumstance (scan rate $V_{SD} = 0.1\ V^{-1}$). The dI/dV value, compared with that of CPNTs, was decreased after immobilization of aptamer on CPNT surfaces; (a) CPNT1 and CPNT1-aptamer, (b) CPNT2 and CPNT2-aptamer. However, the Ohmic contact was retained after the coupling reagent and washing process. This result means that the covalent bonds between CPNTs and gold electrodes can induce reliable electrical contact for FET sensor platform.

phase. Subsequently, 0.25 mmol of P3CA was dissolved in 7.5 mmol of pyrrole and the P3CA/pyrrole mixture was added dropwise into the AOT/hexane mixed solution. The chemical oxidation polymerization of P3CA/pyrrole monomers proceeded through the different temperatures and times of the polymerization [20,27,28]. The resulting products were thoroughly washed with excess ethanol to remove the surfactant (AOT) and other residual reagents. The final products were obtained after drying in a vacuum oven 25 °C. Two kinds of carboxylated polypyrrole nanotubes with diameters of 190–220 nm (CPNT1) and 100–130 nm (CPNT2) were observed by field-emission scanning electron microscopy (FE-SEM). FE-SEM images were taken with a JEOL JSM-6700 F microscope: the samples were coated with a thin layer of gold to eliminate charging effect. In addition, the CPNTs fabricated were p-doped with counterions during chemical oxidation polymerization and the pellet conductivities of the polypyrrole nanotubes by four-probe method were measured to be 10^{-1}–10^{0} S cm^{-1} (CPNT1) and 10^{1}–10^{2} S cm^{-1} (CPNT2).

2.4. Interdigitated electrode array (IDA)

An interdigitated microelectrode array (IDA) was patterned on a glass substrate through a photolithographic process. The IDA consisted of a pair of gold interdigitated microelectrode bands with 25 fingers each, in which the bands served as source (S) and drain (D) electrodes, respectively. The IDA was 2 μm wide, 1 mm length, and had 30 nm thickness (thickness Au 20 nm/Ti 10 nm). The microelectrode substrate was treated with 5 wt% aqueous (3-aminopropyl)trimethoxysilane solution for 6 h in order to introduce amino groups (–NH_2) for binding carboxyl groups (–COOH) of CPNTs.

2.5. Fabrication of sensor platform based on CPNTs-aptamer

An IDA was patterned on a glass substrate by a lithographic process. In order to construct the FET sensor platform, in the first stage, the IDA substrate was treated with 5 wt% aq. (3-aminopropyl)trimethoxysilane (APS) solution for 6 h (Reaction 1) and then exposed to the mixture of 1 wt% CPNT ethanol solution (10 μL) and 1 wt% DMT-MM ethanol solution (40 μL) for 12 h (Reaction 2). The resulting CPNT-immobilized substrate was rinsed with distilled water. Consecutively, the coupling reaction to attach anti-VEGF RNA aptamer onto the CPNT surface was performed by the mixture of anti-VEGF RNA aptamer (10 nM) and 1 wt% DMT-MM aqueous solution (40 μL) for 12 h (Reaction 3). Afterwards, the FET sensor substrate was rinsed with distilled water and dried with a stream of nitrogen gas (Fig. 1);

Reaction 1.

Hydrolysis:

$$H_2N(CH_2)_3Si(OCH_3)_3 + 3H_2O \rightarrow {}_2N(CH_2)_3Si(OH)_3 + 3CH_3OH$$

Condensation:

$$H_2N(CH_2)_3Si(OH)_3 + 3OH - \text{substrate} \rightarrow H_2N(CH_2)_3Si(O)_3 - \text{substrate}$$

Reaction 2. *Condensation*:

$$\text{pyrrole} - COOH + H_2N(CH_2)_3Si(O)_3 - \text{substrate} \rightarrow \text{pyrrole} - CONH(CH_2)_3Si(O)_3 - \text{substrate}$$

Reaction 3. *Condensation*:

$$\text{pyrrole} - COOH + H_2N - \text{anti} - \text{VEGF RNA aptamer} \rightarrow \text{pyrrole} - CONH - \text{anti} - \text{VEGF RNA aptamer}$$

2.6. Fabrication of FET-type biosensor based on CPNTs-aptamer

The synthesized anti-VEGF aptamer conjugated CPNTs (CPNTs-aptamer) geometry as conductive channel of FET was constructed with using a phosphate-buffered solution (10 mM, pH 7.4) as a liquid gate, which was a FET-type sensor for detecting VEGFs (Fig. 2). A solution chamber (volume 70 μL) was designed and employed for all solution-based measurements .The Ag/AgCl reference electrode (R) and Pt counter electrode (C) were immersed in the buffered aqueous solution to provide gate control. The electrolyte-gated transistors have been utilized widely for chemo- and bio-sensing purposes because a three-terminal transistor composed of drain, source, and gate electrodes provides not only an excellent platform for in-depth investigations of gating effects, but also the field-induced modulation (on/off current ratio) of conducting materials [31]. To characterize FET-type sensor based on the CPNTs-aptamer, the gate potential (E_G) was applied relative to between Ag/AgCl 3 M NaCl standard reference electrode and the source electrode through the buffer solution and the current (I_{SD}) between source and drain was measured. The V_{SD} and E_G were confined at low values to rule out the electrochemical side reactions associated with the polymer/electrode or the electrolyte/polymer and the I_{SD} modulation by anti-VEGF aptamer/VEGF binding events was monitored in real-time. All sensing experiments were performed at $V_{SD} = 50$ mV and $E_G = 50$ mV based on the I_{SD}–V_{SD} curves of the CPNTs-aptamer for the gate potential (E_G). From this point of view, it can be explained that the observed current changes in our FET system were due to the charge-transport behavior of the CPNTs elicited by the anti-VEGF aptamer/VEGF binding event.

2.7. The electrical measurement of sensitivity in FET-type sensor

All electrical measurements were conducted with a Keithley 2400-sourcemeter and a Wonatech WBCS 3000 potentiostat. A solution chamber was designed and used for solution-based measurements. The current change was normalized as $[\Delta I/I_0]_{SD} = (I - I_0)/I_0$, where I_0 was the initial current and I was the measured real-time current. The response time was defined as the time required for sensor signal to reach 95% of the maximum value (sensitivity).

3. Results and discussion

3.1. Characterization of size-controlled CPNTs

One-dimension (1D) FET sensor based on conducting nanomaterials can provide the high sensitivity, specificity and label-free electrical readout scheme. In particular, the sensitivity of FET biosensor might be dependent on the shape, conductivity and size in 1D nanomaterials as conductive channel of FET. Under our experimental conditions, we fabricated the CPNTs with diameters of 190–220 nm (CPNT1) and 100–130 nm (CPNT2) by adjusting the

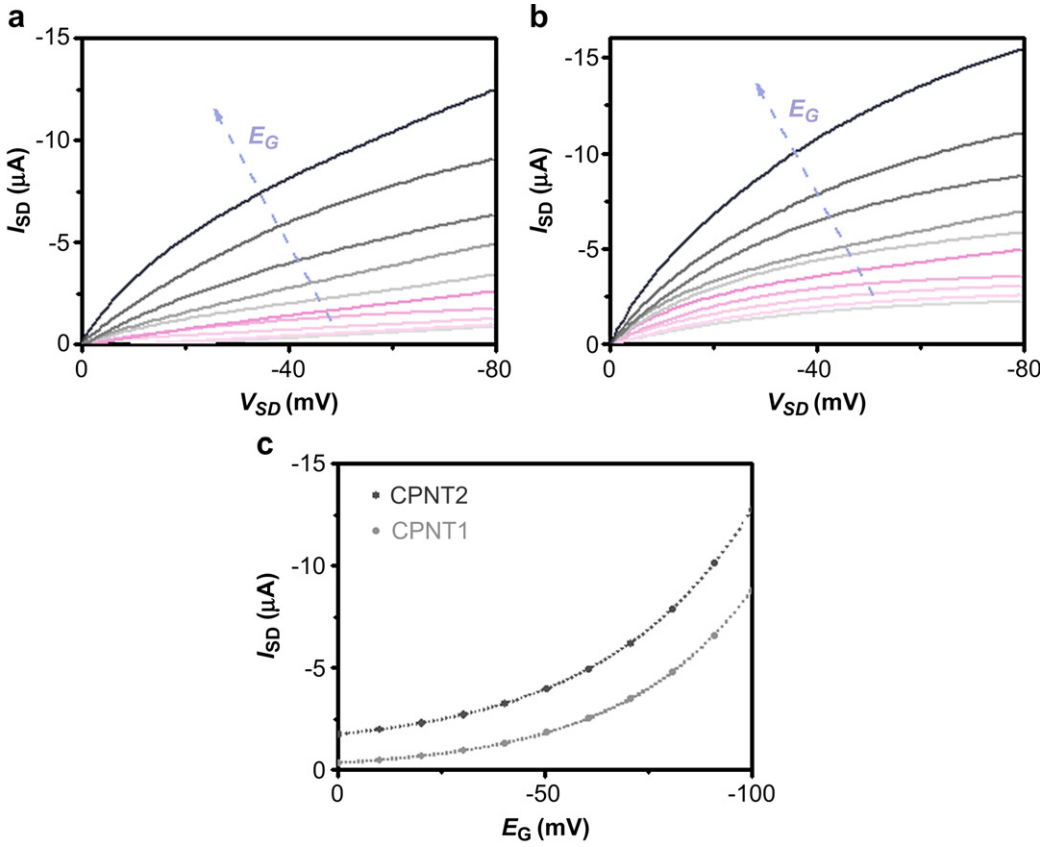

Fig. 5. I_{SD}–V_{SD} characterization of (a) CPNT1-aptamer and (b) CPNT2-aptamer FET sensors for varying E_G from 0 to −100 mV in −10 mV steps (source-drain voltage sweep rate = 10 mV^{-1}). (c) I_{SD}–E_G characteristics of CPNT1-aptamer and CPNT2-aptamer FET sensors for a constant V_{SD} = −50 mV.

polymerization time and temperature because the sensitivity of conducting polymer transducer increase with increasing the surface area. The pellet conductivities measured by four-probe method were 10^{-1}–10^{0} S cm^{-1} (CPNT1) and 10^{1}–10^{2} S cm^{-1} (CPNT2), respectively. The conductivity of CPNT2 was higher than those of CPNT1 due to the nano-effect [20].

3.2. Characterization of FET sensor platforms with CPNTs

To confirm the sensing ability of CPNT1 and CPNT2 in the FET, they were attached by the chemical reaction on the glass substrate treated with APS and used as a conductive channel of FET sensor. The carboxyl functional groups (−COOH) of CPNTs were coupled with the amino groups ($-NH_2$) of the IDA substrate surfaces via a condensation reaction. Compared with conventional lithographic methods, this immobilization approach offers critical advantages such as mild reaction conditions and a simple process for the successful integration of CPNTs into the electrode substrate [32]. Fig. 3 displays typical field-emission scanning electron microscopy (FE-SEM) images of FET sensor platform with CPNT1 and CPNT2 on the IDA substrate. From FE-SEM analysis, the CPNT1 had an average diameter of 200 nm and CPNT2 had an average diameter of 120 nm. It was clearly observed that CPNT1-aptamer (Fig. 3b) and CPNT2-aptamer (Fig. 3d) were considerably made more rugged by the attached anti-VEGF RNA aptamer by comparison with pristine CPNT1 (Fig. 3a) and CPNT2 (Fig. 3c). Moreover, there was no aptamers on the electrode substrate except on the CPNTs, thus indicating that the aptamer was selectively deposited on the CPNTs through chemical coupling. Furthermore, covalent anchoring provides better stability for analyte sensing in the liquid phase [21].

In the case of biosensor, sensitivity measurement was carried out in the liquid phase for detecting the bio-molecules as analytes. This can be affected by the surrounding medium in the liquid phase when CPNTs/IDA substrate and CPNTs/anti-VEGF aptamer were combined by physical connections. Moreover, compared with a non-covalent approach, covalent bonding formation provides better stability for analyte sensing in the liquid phase and further offers the possibility to control the chemical functionality of the CPNTs [29]. Therefore, the covalent bonding between anti-VEGF RNA aptamer and the CPNTs surface was reduced through a condensation reaction. To evaluate the quality of the electrical contact after introduction of anti-VEGF aptamers on the CPNTs surface, the I–V characteristics of FET sensor platform with CPNTs were investigated. Fig. 4 indicates current–voltage (I–V) curves of CPNT1 and CPNT2 before and after immobilization of anti-VEGF aptamer in air (scan rate V_{SD} = 0.1 V^{-1}). The dI/dV value of the pristine CPNT1 was as high as 11.527×10^{-6} S. This value slightly decreased to 5.842×10^{-6} S after anti-VEGF aptamer immobilization (Fig. 4a). The dI/dV value of the pristine CPNT2 was 17.257×10^{-6} S, and that of the aptamer-immobilized CPNT2 (8.842×10^{-6} S) was calculated less than pristine CPNT2 (Fig. 4b). Moreover, the dI/dV values of CPNT2 and CPNT2-aptamer were higher than those of the CPNT1 and CPNT1-aptamer. This result can be explained by their conductivity (CPNT2 > CPNT1) and size-effect (CPNT2 < CPNT1). In the case of connection between gold electrode and CPNTs, there are two mechanisms of the current flows; one is Ohmic contact and the other is Schottky contact [32]. The two I–V plots in the Fig. 4 appeared to be linear, representing an excellent Ohmic contact characteristic. To immobilize the anti-VEGF aptamer on the CPNTs surface under our experimental condition, CPNTs inevitably reacted with aptamer during condensation process,

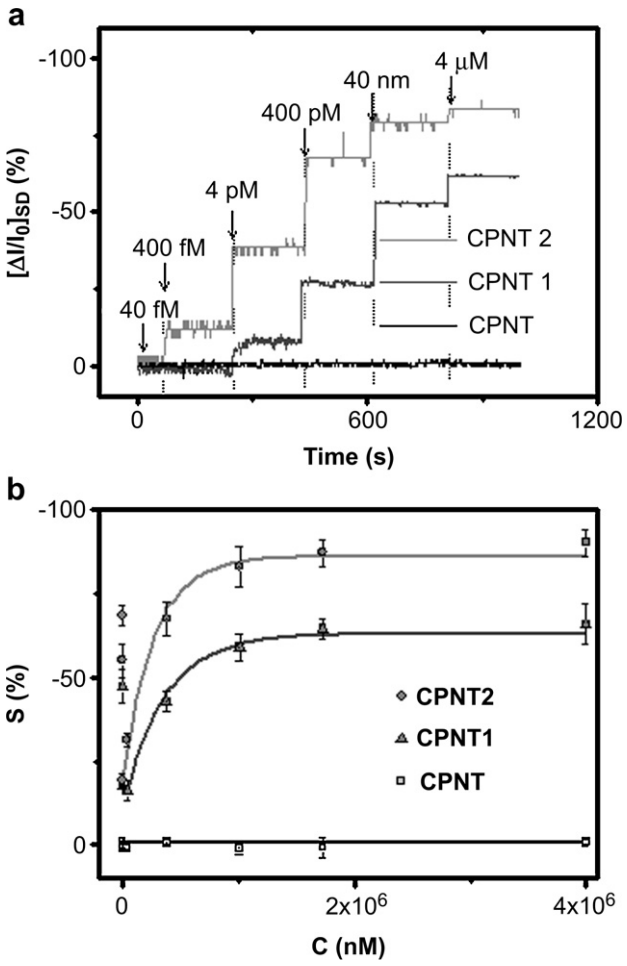

Fig. 6. (a) Real-time response and (b) calibration curves of anti-VEGF aptamer conjugated CPNT1 and CPNT2 FET sensors toward VEGFs with various concentrations (V_{SD} = −50 mV). The detection limit of VEGF concentrations was near 400 fM. The linear increase in sensitivity under 4 μM was observed and the sensitivity was saturated at higher values.

followed by a washing step with distilled water. The oxidation level of CPNTs may be affected by the chemicals and the doped counterions can be physically detached from the polymer backbone during this washing process. Consequently, it is believed that this

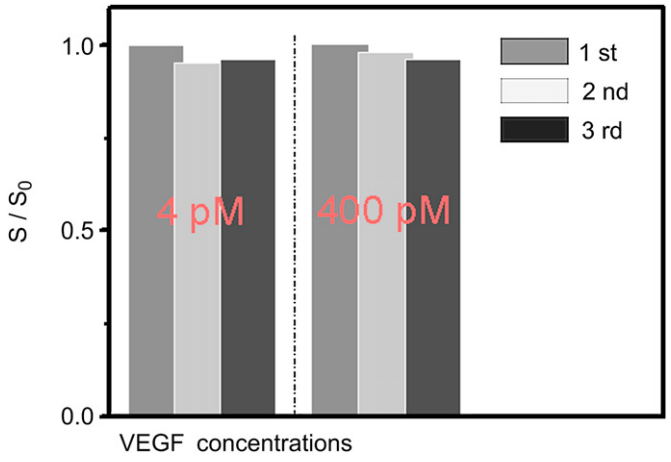

Fig. 7. A re-useable CPNT1-aptamer FET sensor system; the sensitivity changes were calculated through the consecutive assay of three times at 4 pM and 400 pM concentrations of VEGF (the sensitivity change was calculated as S/S_o, where S_o is the initial sensitivity and S is the measured sensitivity after washing and rinsing process).

immobilization procedure played a role in causing a change in the dI/dV value. Nevertheless, the linearity in I–V characteristic was still maintained after introduction of anti-VEGF aptamer toward CPNTs surfaces and the dI/dV values were also maintained within the same order of magnitude. Therefore, it can be considered that anti-VEGF aptamer molecules are effectively incorporated into CPNTs without any drastic loss in electrical contact and conductivity. Furthermore, these results provide the reliable electrical contact at the CPNTs/gold electrode interface through the covalent immobilization.

3.3. Characterization of FET sensor based on CPNTs-aptamer

In order to investigate suitable FET characteristics to detect charged bio-molecules, FET sensors based on CPNT1-aptamer and CPNT2-aptamer were measured as a function of source-drain current (I_{SD}) versus source-drain voltage (V_{SD}). FET sensor platform with CPNTs-aptamer was surrounded by PBS (pH 7.4) as liquid gate and constituted to three electrolyte-gated transistors (Fig. 2). To confirm the sensing capability of FET sensor to detect analyte, the basic voltage (V_{SD}) was continuously applied to the source (S) electrode with respect to the drain (D) electrodes. The gate potential (E_G) was also provided through the Ag/AgCl reference electrode (R) across CPNTs to vary the electrostatic potential of CPNTs as conductive channels immersed in liquid gate. Fig. 5 displays the dependence of source-drain current (I_{SD}) versus source-drain voltage (V_{SD}) for varying E_G (E_G was applied from 0 V to −100 mV and step −10 mV, source-drain voltage sweep rate was 10 mV^{-1}) in a PBS buffer solution. The I_{SD} modulations of CPNT1 (Fig. 5a) and CPNT2 (Fig. 5b) increased gradually with increasing negative E_G at a negative V_{SD}, indicating the electrical characteristic of p-type accumulation mode. Fig. 5c displays a plot of I_{SD} versus E_G at a constant drain voltage (a representative value of $V_{SD} = -50$ mV) for the p-type FET sensor. These results mean that the negative E_G gives rise to an increase in the oxidation level of CPNT chain. Therefore, CPNTs-aptamer sensor can represent the p-type FET characteristic in the doped state [32]. Furthermore, potential variations were originated from affinity between CPNTs-aptamer and analyte (bio-molecules) in FET system, which could affect the I_{SD} in a similar manner to the effect of applying E_G. Consequently, the dependence of I_{SD} on the various E_G demonstrates that this FET sensor is efficiently employed as the electrochemical biosensor for detecting charged bio-molecules in solution.

3.4. Real-time responses of FET sensor based on CPNTs-aptamer toward VEGF

To identify the performance of the FET sensor fabricated, we measured the current changes of FET sensors as a function of various VEGF concentrations in the real time at constant V_{SD}. These FET sensors were surrounded by the glass chamber to minimize environment effect and the PBS solution as liquid gate was droplet through the glass chamber. The various amount of VEGF was consecutively added into the glass chamber. The identical experiment was also performed with using a CPNT FET sensor without anti-VEGF aptamer. Fig. 6a displays the real-time responses of CPNT1-aptamer, CPNT2-aptamer and pristine CPNTs FET sensors with respect to the various concentrations of the VEGF (V_{SD} = −50 mV). The responses reflected the normalized current changes which were calculated as $[\Delta I/I_0]_{SD}$ (%) = $(I - I_0)/I_0 \times 100$ (where I_0 was the initial current and I was the measured real-time current). When the FET sensor was exposed to the various VEGF solutions, CPNTs-aptamer sensor exhibited a fast response (<1 s) in real-time. The current values in this FET system decreased with increasing VEGF concentrations by molecule-gating effects arising from adding VEGF concentrations (Fig. 5). Specifically, VEGFs have

the isoelectric point (p*I*) values of ranging near 8.5 and are positively charged under the experimental condition of pH 7.5. These positively charged VEGFs can interact with anti-VEGF aptamer on the CPNT, resulting in accumulating the negative charge on the CPNT surfaces. Therefore, the increasing negative charges diminish p-doing effect in the CPNTs, which is probably responsible for the decrease in I_{SD}. Fig. 6b represents calibration curve of the CPNT1-aptamer and CPNT2-aptamer FET sensors toward VEGF with different concentrations. The sensitivity (S) was determined from the normalized I_{SD} changes. The saturation in the sensitivity was observed over 4 μM. Importantly, the detection limit of CPNT1-aptamer FET sensor was found to be 4 pM, approximately two orders of magnitude lower than that of VEGF sensor based on Si nanowire FETs [11]. Furthermore, that of the CPNT2-aptamer FET-type sensor showed the highest performance (400 fM) due to the smaller dimensions, the enhanced surface area and higher conductivity compared with CPNT1. In particular, the sensitivity of CPNT2-aptamer was approximately as twice as that of CPNT1 at low concentrations.

3.5. A re-useable CPNTs-aptamer FET sensor system

Main advantage of this FET sensor system is that each FET-platform including CPNT1-aptamer and CPNT2-aptamer can be repeatedly used for various concentrations of the target molecule (VEGF). In order to use CPNTs-aptamer sensor repeatedly, the washing and rinsing processes are needed inevitably. These processes are composed of three steps: washing dilute sodium chloride solution, rinsing with DEPC-treated water and air dry. Used FET-platform was refreshed and reused for another sample assay. Fig. 7 demonstrates a re-useable CPNTs-aptamer FET sensor system (the sensitivity changes were calculated as S/S_o, where S_o is the initial sensitivity and S is the measured sensitivity after the washing and rinsing processes). The CPNT1-aptamer FET sensor was successfully reused for the consecutive assay of three times at 4 pM and 400 pM concentrations of VEGF. Each consecutive assay represented reproducible and consistent signals for all the samples tested. The CPNT2-aptamer FET sensor also showed same results.

4. Conclusion

We have demonstrated the feasibility of high-performance FET-type sensor based on CPNTs conjugated with anti-VEGF aptamer as transducer. The chemical immobilization strategy between CPNTs and anti-VEGF aptamer provided the various advantages such as the facile fabrication of the *p*-type FET sensor, an environmental stability in the aqueous solution, and superior conductivity of FET substrate. The CPNTs-aptamer FET sensors displayed the high affinity toward VEGFs and afforded measurable signals as low as 400 fM of analyte concentration in real-time. Moreover, this FET sensor demonstrated reproducible and reversible characteristics through washing and rising processes. Therefore, this CPNTs-aptamer FET biosensor can provide a label-free, convenient and sensitive method to recognize target molecule in real time. Furthermore, this methodology offers a route to the fabrication of highly sensitive devices for the efficient diagnosis of cancer in real-time.

Acknowledgements

This research was supported by a grant from the Center for Advanced Materials Processing (CAMP) of the 21st Century Frontier R&D Program funded by the Ministry of Knowledge Economy (MKE), Republic of Korea and the WCU (World Class University) program through the National Research Foundation of Korea funded by the Ministry of Education, Science and Technology (R31-10013).

Appendix

Figures with essential color discrimination. Figs. 1, 2, 5 and 7 in this article are difficult to interpret in black and white. The full color images can be found in the on-line version, at doi:10.1016/j.biomaterials.2010.02.040.

References

[1] Suzuki Y, Yokoyama K. Development of a fluorescent peptide for the detection of vascular endothelial growth factor (VEGF). ChemBioChem 2009;10:1793–5.
[2] Brahimi-Horn MC, Pouyssegur J. Oxygen, a source of life and stress. FEBS Lett 2007;581:3582–91.
[3] Loureiro RMB, D'Amore PA. Transcriptional regulation of vascular endothelial growth factor in cancer. Cytokine Growth Factor Rev 2005;16:77–89.
[4] Foekens JA, Peters HA, Grebenchtchikov N, Look MP, Meiger-Van Gelder ME, Geurts-Moespot A. High tumor levels of vascular endothelial growth factor predict poor response to systemic therapy in advanced breast cancer. Cancer Res 2001;15:5407–14.
[5] Wang HU, Chen Z-F. Molecular distinction and angiogenic interaction between embryonic arteries and veins revealed by ephrin-B2 and its receptor Eph-B4. Cell 1998;93:741–53.
[6] Vikkula V, Boon LM, Carraway III KL, Calvert JT, Diamonti AJ, Goumnerov B, et al. Vascular dysmorphogenesis caused by an activating mutation in the receptor tyrosine kinase TIE2. Cell 1996;87:1181–90.
[7] Ferrara N, Gerber HP, LeCouter J. The biology of VEGF and its receptors. Nat Med 2003;92:3566–70.
[8] Langer I, Vertongen P, Perret J, Fontaine J, Atassi G, Robberecht P. Expression of vascular endothelial growth factor (VEGF) and VEGF receptors in human neuroblastomas. Med Pediatr Oncol 2000;34:386–93.
[9] Ferrara N. Vascular endothelial growth factor: basic science and clinical progress. Endocr Rev 2004;25:581–611.
[10] Poh CK, Shi Z, Lim TY, Neoh KG, Wang W. The effect of VEGF functionalization of titanium on endothelial cells in vitro. Biomaterials 2009;31:1578–85.
[11] Lee H-S, Kim KS, Kim C-J, Hahn SK, Jo M-H. Electrical detection of VEGFs for cancer diagnoses using anti-vascular endothelial growth factor aptamer-modified Si nanowire FETs. Biosens Bioelectron 2009;24:1801–5.
[12] Sung J, Barone PW, Kong H, Strano MS. Sequential delivery of dexamethasone and VEGF to control local tissue response for carbon nanotube fluorescence based micro-capillary implantable sensors. Biomaterials 2009;30:622–31.
[13] Anderson SM, Chen TT, Iruela-Arispe ML, Segura T. The phosphorylation of vascular endothelial growth factor receptor-2 (VEGFR-2) by engineered surfaces with electrostatically or covalently immobilized VEGF. Biomaterials 2009;30:4618–28.
[14] Prabhulkar S, Alwarappan S, Liu G, Li C-Z. Amperometric micro-immunosensor for the detection of tumor biomarker. Biosens Bioelectron 2009;24:3524–30.
[15] Williams DF. On the nature of biomaterials. Biomaterials 2009;30:5890–7.
[16] Lee J-O, So H-M, Jeon E-K, Chang H, Won K, Kim YH. Aptamers as molecular recognition elements for electrical nanobiosensors. Anal Bioanal Chem 2008;390:1023–32.
[17] Binga T, Liua X, Chenga X, Caoa Z, Shangguana D. Bifunctional combined aptamer for simultaneous separation and detection of thrombin. Biosens Bioelectron 2010;25:1487–92.
[18] Guoa K-T, Scharnweberb D, Schwenzerc B, Ziemera G, Wendela HP. The effect of electrochemical functionalization of Ti-alloy surfaces by aptamer-based capture molecules on cell adhesion. Biomaterials 2007;28:468–74.
[19] Wu Z-S, Zheng F, Shen G-L, Yu R-Q. A hairpin aptamer-based electrochemical biosensing platform for the sensitive detection of proteins. Biomaterials 2009;30:2950–5.
[20] Yoon Y, Jang J. Conducting-polymer nanomaterials for high-performance sensor applications: issues and challenges. Adv Funct Mater 2009;19:1567–76.
[21] Kwon OS, Hong T-J, Kim SK, Jeong J-H, Hahn JS, Jang J. Hsp90-functionalized polypyrrole nanotube FET sensor for anti-cancer agent detection. Biosens Bioelectron 2010;25:1307–12.
[22] Jang J. Conducting polymer nanomaterials and their applications. Adv Polym Sci 2006;199:189–90.
[23] Yoon H, Jang J. Versatile strategies for fabricating polymer nanomaterials with controlled size and morphology. Macromol Res 2008;16:85–102.
[24] Korri-Youssoufi H, Garnier F, Srivastava P, Godillot P, Yassar AH. Toward bioelectronics: specific DNA recognition based on an oligonucleotide-functionalized polypyrrole. J Am Chem Soc 1997;119:7389–99.
[25] Garnier F, Youssoufi HK, Srivastava P, Yassar A. Enzyme recognition by polypyrrole functionalized with bioactive peptides. J Am Chem Soc 1994;116:8813–4.

[26] Potyrailo RA. Polymeric sensor materials: toward an alliance of combinatorial and rational design tools? Angew Chem Int Ed 2006;45:702–23.
[27] Yoon H, Ko S, Jang J. Field-effect-transistor sensor based on enzyme-functionalized polypyrrole nanotubes for glucose detection. J Phys Chem B 2008;112:9992–7.
[28] Yoon H, Lee SH, Kwon OS, Song HE, Oh EH, Park TH, et al. Polypyrrole nanotubes conjugated with human olfactory receptors: high-performance transducers for FET-type bioelectronic noses. Angew Chem Int Ed 2009;48:2755–8.
[29] Willner I. Electronic aptamer-based sensors. Angew Chem Int Ed 2007; 46:6408–18.
[30] Kunishima M, Kawachi C, Hioki K, Terao K, Tani S. Formation of carboxamides by direct condensation of carboxylic acids and amines in alcohols using a new alcohol- and water-soluble condensing agent: DMT-MM. Tetrahedron 2001;57:1551–8.
[31] Alam MM, Wang J, Guo Y, Lee SP, Tseng H-R. Electrolyte-gated transistors based on conducting polymer nanowire junction arrays. J Phys Chem B 2005;109:12777–84.
[32] Yoon H, Kim J-H, Lee N, Kim B-G, Jang J. A novel sensor platform based on aptamer-conjugated polypyrrole nanotubes for label-free electrochemical protein detection. ChemBioChem 2008;9:634–41.